AD-A146 700 X-RAY PRODUCTION IN LONG-SCALELENGTH LASER-PLASMA 1/1
INTERACTION EXPERIMENTS(U) NAVAL RESEARCH LAB
WASHINGTON DC F C YOUNG ET AL. 04 NOV 83 NRL-MR-5174
UNCLASSIFIED DE-AI08-79DP40092 F/G 20/6 NL

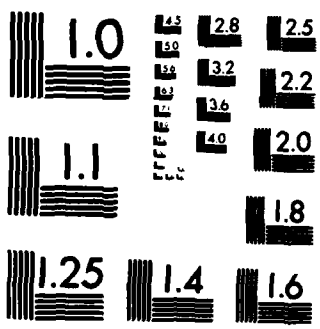

(2)

NRL Memorandum Report 5174

X-Ray Production in Long-Scalelength Laser-Plasma Interaction Experiments

F. C. YOUNG, M. J. HERBST, J. H. GARDNER,* K. J. KEARNEY,** J. A. STAMPER, S. P. OBENSCHAIN, J. GRUN,** E. A. MCLEAN AND B. H. RIPIN

Laser Plasma Branch
Plasma Physics Division

**Laboratory for Computational Physics*

***Mission Research Corporation*
Alexandria, VA 22312

November 4, 1983

This work was supported by the U.S. Department of Energy.

This report was prepared for presentation at the Thirteenth Annual Anomalous Absorption Conference held in Banff, Canada, June 5-10, 1983.

NAVAL RESEARCH LABORATORY
Washington, D.C.

SECURITY CLASSIFICATION OF THIS PAGE (When Data Entered)

REPORT DOCUMENTATION PAGE	READ INSTRUCTIONS BEFORE COMPLETING FORM
1. REPORT NUMBER NRL Memorandum Report 5174	2. GOVT ACCESSION NO. AD-A146700	3. RECIPIENT'S CATALOG NUMBER
4. TITLE (and Subtitle) X-RAY PRODUCTION IN LONG-SCALELENGTH LASER-PLASMA INTERACTION EXPERIMENTS		5. TYPE OF REPORT & PERIOD COVERED Interim report on a continuing NRL problem. 6. PERFORMING ORG. REPORT NUMBER
7. AUTHOR(s) F.C. Young, M.J. Herbst, J.H. Gardner, K.J. Kearney,* J.A. Stamper, S.P. Obenschain, J. Grun,* E.A. McLean and B.H. Ripin		8. CONTRACT OR GRANT NUMBER(s)
9. PERFORMING ORGANIZATION NAME AND ADDRESS Naval Research Laboratory Washington, DC 20375		10. PROGRAM ELEMENT, PROJECT, TASK AREA & WORK UNIT NUMBERS DE-AI08-79DP40092; 47-0859-0-3
11. CONTROLLING OFFICE NAME AND ADDRESS U.S. Department of Energy Office of Inertial Fusion Washington, DC 20545		12. REPORT DATE November 4, 1983 13. NUMBER OF PAGES 13
14. MONITORING AGENCY NAME & ADDRESS(if different from Controlling Office)		15. SECURITY CLASS. (of this report) UNCLASSIFIED 15a. DECLASSIFICATION/DOWNGRADING SCHEDULE

16. DISTRIBUTION STATEMENT (of this Report)

Approved for public release; distribution unlimited.

17. DISTRIBUTION STATEMENT (of the abstract entered in Block 20, if different from Report)

18. SUPPLEMENTARY NOTES

*Present address: Mission Research Corporation, Alexandria, VA 22312

This work was supported by the U.S. Department of Energy.
This report was prepared for presentation at the Thirteenth Annual Anomalous Absorption Conference held in Banff, Canada, June 5-10, 1983.

19. KEY WORDS (Continue on reverse side if necessary and identify by block number)

Laser-produced plasma
Long-scalelength plasma
Thermal electron temperature
Hot electron temperature
Hot electron thresholds
Hot electron intensity

20. ABSTRACT (Continue on reverse side if necessary and identify by block number)

The interaction of a high intensity laser beam ($I > 10^{14}$ W/cm^2) with long-scalelength plasmas ($|n_e/\nabla n_e| \leq 400$ μm at 0.1 critical density) is being studied experimentally by using two beams from the Pharos II Nd laser ($\lambda = 1.054$ μm). A low-intensity defocused beam of 4-nsec duration produces background plasmas of variable scalelength from a solid plastic target. A 0.3-nsec focused beam timed to arrive on target near the peak of the long pulse interacts with this long-scalelength plasma. Temporally and spatially integrated bremsstrahlung intensities from 1 to 50 keV are measured.

(Continues)

DD FORM 1 JAN 73 1473 EDITION OF 1 NOV 65 IS OBSOLETE
S/N 0102-014-6601

SECURITY CLASSIFICATION OF THIS PAGE (When Data Entered)

20. ABSTRACT (Continued)

X-ray spectra deduced from the measurements are used to evaluate target heating (based on 1-5 keV x-rays) and to determine the relative importance of energetic electron production by plasma instabilities in the underdense region (based on 10-50 keV x-rays).

The thermal x-ray emission is dominated by the higher energy 4-nsec laser pulse and corresponds to electron temperatures of about 300 eV. The intensity of this emission scales with the laser energy, as expected. Temperatures determined from these measurements are compared with those extracted using time-resolved x-ray diagnostics. Also, temperatures are compared with values extracted from bremsstrahlung spectra based on a 2-D hydrocode analysis of this experiment.

The dependence of the intensity of energetic x-ray emission and the associated hot electron temperature, T_h, on the background plasma scalelength and the energy of the short pulse are reported. Values of T_h range from 6 to 10 keV, and variations in the energetic x-ray intensity of more than an order of magnitude are observed in the experiment. For low energy in the short pulse, the energetic x-ray emission increases with background plasma scalelength, but this behavior is not maintained as the energy is increased. These observations suggest that the energetic electrons are produced by different plasma instabilities at low energy and at high energy.

X-RAY PRODUCTION IN LONG-SCALELENGTH LASER-PLASMA INTERACTION EXPERIMENTS

Measurements of x-rays produced in longer-scalelength interaction experiments carried out using the NRL Pharos II Nd laser facility are described in this presentation. The configuration of the laser and the target for these experiments is shown in Fig. 1. A 4-ns laser pulse is used to irradiate a large area on target to create a long-scalelength background plasma. A 0.3-ns laser pulse, timed to the peak of the long pulse, is focused to a smaller area and at higher irradiance to study the laser-plasma interaction. The x-ray emission is evaluated in terms of two experimental parameters: background-plasma scalelength and short-pulse laser intensity. The background-plasma scalelength is varied by changing the larger spot size at constant irradiance. Measurements were carried out at three different spot sizes which correspond to short, medium and long scalelength conditions. These conditions correspond to scalelengths of 140, 240 and 320 μm, respectively, at one-quarter critical density. The laser intensity is varied by changing the short-pulse energy. Bremsstrahlung radiation from 1 to 50 keV is measured in order to evaluate the background-plasma temperature, the perturbed-plasma temperature and energetic electron production by the short-pulse focused beam.

The background and perturbed plasma temperatures are determined by time-resolving the thermal x-ray emission. The background-plasma temperature corresponds to heating by the long pulse only while the perturbed plasma temperature is due to heating by the short laser pulse. Traces from two detectors with filters designed to detect 1-1.5 keV (Aℓ) and 2-2.8 keV (Cl) x rays respectively are presented in Fig. 2. Each detector consists of a quenched plastic scintillator coupled to a vacuum photodiode giving an overall time response of ~ 0.7 ns. Both detectors record x rays from the short pulse and the long pulse. The relative amplitudes of the responses in the two detectors are used to determine the temperatures given in Fig. 2. These temperatures are based on a thermal Maxwellian electron energy distribution. The long-pulse response is time-resolved, and the background plasma temperatures, evaluated at maximum x-ray emission, are determined to ± 10%. These detectors integrate the short pulse so the perturbed-plasma temperatures are time-averaged. Consequently, these values represent lower limits on the heating of the perturbed plasma. The spread in values of the perturbed-plasma temperatures encompass the variation in short-pulse laser energy.

Manuscript approved September 15, 1983.

The measured temperatures are compared to temperatures determined from hydrodynamic modeling of the experiment.[1] The free-bound x-ray radiation is evaluated using density and temperature profiles given by the hydro-code, and the slope of the 1-3 keV x-ray region is used to extract the temperature after appropriate spatial and temporal integration. Temperatures determined with the hydro-code are shown in parentheses in Fig. 2. These results are consistently higher than the experiment. This may be due to the fact that the code does not include refraction of the incident light in the underdense region. Only a small amount of refraction would be required to increase the heated target area by the 10% needed to explain the discrepancy. Also, laser energy could be absorbed in the underdense region by processes other than inverse bremsstrahlung and would not be accounted for in the hydro-code calculations.

Results from temporally and spatially integrated x-ray measurements will be presented in the remainder of this report. Typical x-ray spectra are shown in Fig. 3. Detector arrays with K-edge filters are used: PIN diodes for the low energy region (1-10 keV) and scintillator-photomultipliers for the high energy region (20-50 keV). The two spectra in Fig. 3 are for a fixed short scalelength but different short-pulse laser energies. The low energy x-ray emission is characterized by a thermal electron temperature (T_e) and is dominated by the 4-ns long pulse so these two low energy spectra are quite similar. The high energy x-ray emission is characterized by a hot electron temperature (T_h) and a total energy (E_{20}) corresponding to the integrated emission above 20 keV. This emission is sensitive to the short-pulse energy. At low energy, the x-ray emission is less than experimental detection limits as shown by the dashed line in Fig. 3. The long laser pulse gives no detectable high energy emission because it is at low irradiance. We shall see later that this high energy emission does increase with scalelength as well as with laser energy as evidenced in Fig. 3. Results for T_e, T_h and E_{20} respectively, are presented in the next three figures.

Thermal electron temperatures (T_e) at the short, medium and long scalelengths are presented in Fig. 4. The temperature is nearly constant at 300 eV because the irradiance is held nearly constant as the scalelength is changed. For the medium and long scalelengths, a weak dependence on long-pulse laser energy is evident. At short scalelength, the energy in the short pulse approaches that of the long pulse and thereby introduces scatter in these time-integrated measurements. For comparison, the time-resolved background temperatures presented in Fig. 2 are

indicated by the horizontal lines. These values are consistently higher than the time-integrated results, as one intuitively expects.

Hot electron temperatures (T_h) are given in Fig. 5 as a function of the short-pulse laser energy for all three scalelengths. At low energy and short scalelength no energetic x rays are observed, but increasing either the scalelength or the laser energy causes an onset of energetic x-ray emission (i.e., hot electrons). Values of T_h range from about 6 to 10 keV and have very little dependence on short-pulse energy. Average values at the three scalelengths are indicated in Fig. 5. Here also only a weak dependence on scalelength is seen.

Of more interest is the hot electron population as measured by the integral (E_{20}) of the high energy tail of the x-ray spectrum . This quantity, normalized to the incident laser energy, is displayed in Fig. 6 for the three scalelengths. At short scalelength, the fraction of high energy x rays increases rapidly from an apparent threshold at ~ 10 Joules (corresponding to a vacuum irradiance of 2×10^{14} W/cm^2). Above 20 Joules this fraction increases less rapidly. At longer scalelengths the behavior is quite different. X rays are detected even for laser energies less than 10 Joules and the intensity increases with scalelength. There is a minimum in the intensity near 15 Joules, and above 30 Joules the intensity varies by an order-of-magnitude from shot to shot - even though the hot electron temperature is rather constant. At 7 Joules, for example, a threshold is apparent between short and medium scalelengths. Contrast this behavior to that at 20 Joules where the intensity is nearly constant as the scalelength is increased.

Hot electron fractions were determined from values of E_{20} and T_h, and the results at 7 and 20 Joules are shown in Fig. 7. Hot electron fractions are presented in terms of the focal diameter of the long laser pulse for the three scalelengths, rather than the scalelength, because the scalelength variation is strikingly different at critical density (n_c) and in the underdense region ($n_c/4$) as shown at the top of this figure. These hot electron fractions are based on thick-target bremsstrahlung with the assumption that one-half of the electrons are directed into the target. The increasing hot electron fraction at 7 Joules correlates with the scalelength variation at $n_c/4$, whereas the rather constant hot electron fraction at 20 Joules correlates with the constant scalelength at n_c. Therefore, one is inclined to look for an underdense instability at low energy and a critical-density process at high energy as potential sources for generating energetic electrons. This interpretation is consistent with the experimental

observation that more laser energy does penetrate to the critical surface at high energy.[1,2] However, other explanations are possible; for example, profile steepening at $n_c/4$ due to local energy deposition by an instability could eliminate the differences between the three background plasmas at higher incident energy.

In conclusion, time-resolved x-ray measurements have shown that the perturbed plasma is heated to a temperature of 1.1 to 1.8 times that of the background plasma, depending on the laser energy. Measurements of 20-50 keV x rays have demonstrated that the energetic electron intensity has a threshold with increasing laser energy for short scalelength, and a threshold with increasing scalelength for low laser energy. Also, above threshold the hot electron temperature is 7-9 keV and scales only weakly with plasma scalelength and laser energy. Arguments can be made to support energetic electron production by underdense plasma instabilities at low energy and critical-surface phenomena at high energy. Self-focusing, which was inferred from images of second harmonic emission in this experiment,[3] may impact energetic electron production at the higher energies. However, we cannot make definitive statements regarding mechanisms for energetic electron production at this time.

REFERENCES

1. J.H. Gardner, M.H. Emery, J. Grun, M.J. Herbst, R.L. Lehmberg, E.A. McLean, J.A. Stamper, and F.C. Young, "Hydrodynamic Modeling of Longer-Scalelength Interaction Experiments," presented at 13th Annual Anomalous Absorption Conference, Alberta, Canada, June 5-10, 1983.
2. M.J. Herbst, J. Grun, J.H. Gardner, K.J. Kearney, R.H. Lehmberg, E.A. McLean, S.P. Obenschain, J.A. Stamper, F.C. Young, and B.H. Ripin, "Longer-Scalelength Interaction Experiments: Observations of Scattered Light," ibid.
3. J.A. Stamper, F.C. Young, M.J. Herbst, S.P. Obenschain, J.H. Gardner, R.H. Lehmberg, E.A. McLean, J. Grun, K.J. Kearney, and B.H. Ripin, "Longer-Scalelength Plasma Perturbations by an Intense Laser Beam," ibid.

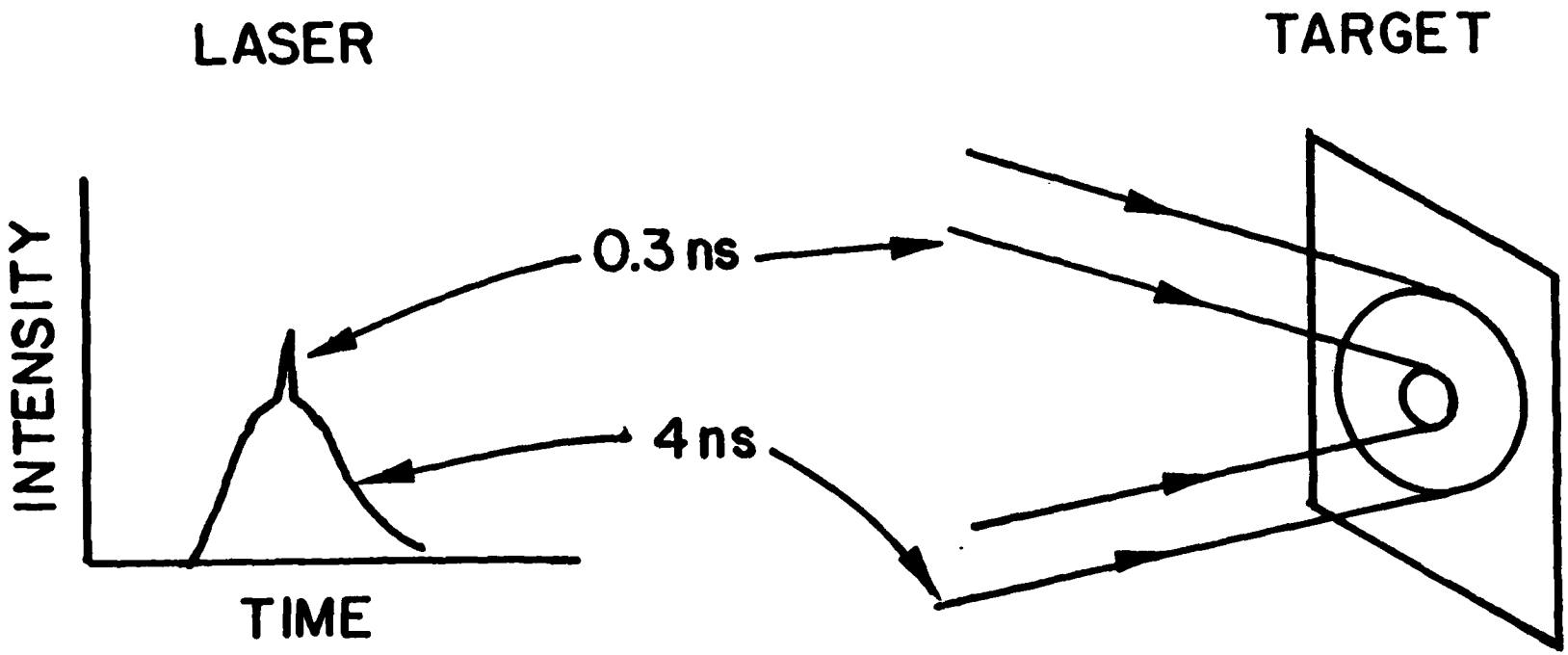

Fig. 1 Configuration of the short (0.3-ns) and long (4-ns) laser pulses for long scalelength interaction experiments. The target is a 150 to 180 μm thick planar polyethylene foil.

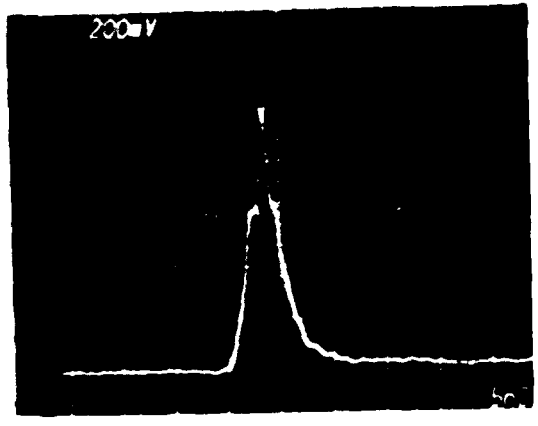

Al Filter (0.25mil)

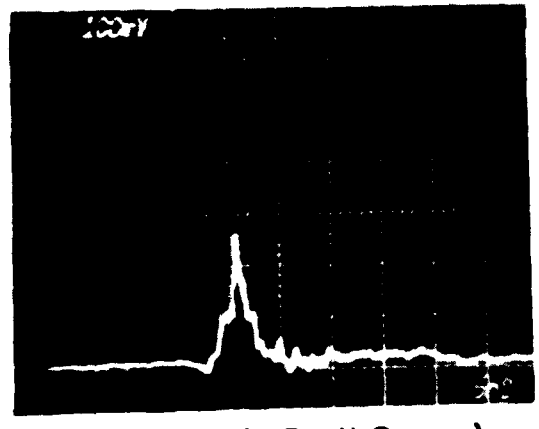

Cl Filter (1.5mil Saran)

Background Scale-lengths	Background Temperatures (long-pulse, time-resolved)	Perturbed Temperatures (short-pulse, time-averaged)
Short	310 eV (360 eV)	320-460 eV (475-520 eV)
Medium	350eV	370-550 eV
Long	370 eV (405 eV)	460-570 eV (510-560 eV)

Fig. 2 Electron temperatures determined from time-resolved thermal x-ray measurements. Traces from detectors with 1.7 mg/cm^2 thick Al and 6 mg/cm^2 thick Saran ($H_2C_2Cl_2$) filters are also shown.

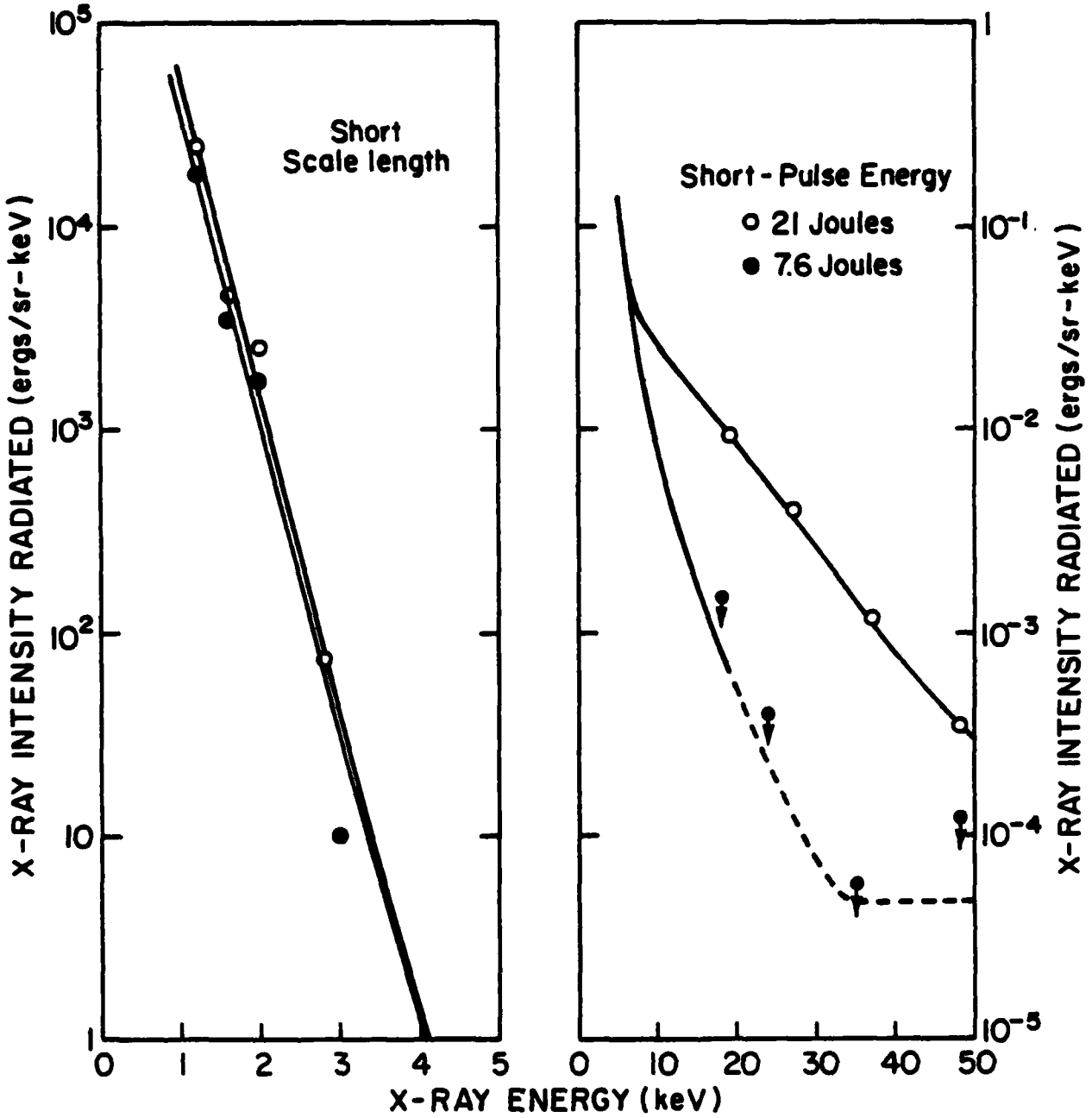

Fig. 3 Typical temporal and spatially integrated x-ray spectra for the short scalelength condition. The points with arrows correspond to experimental limits of detection.

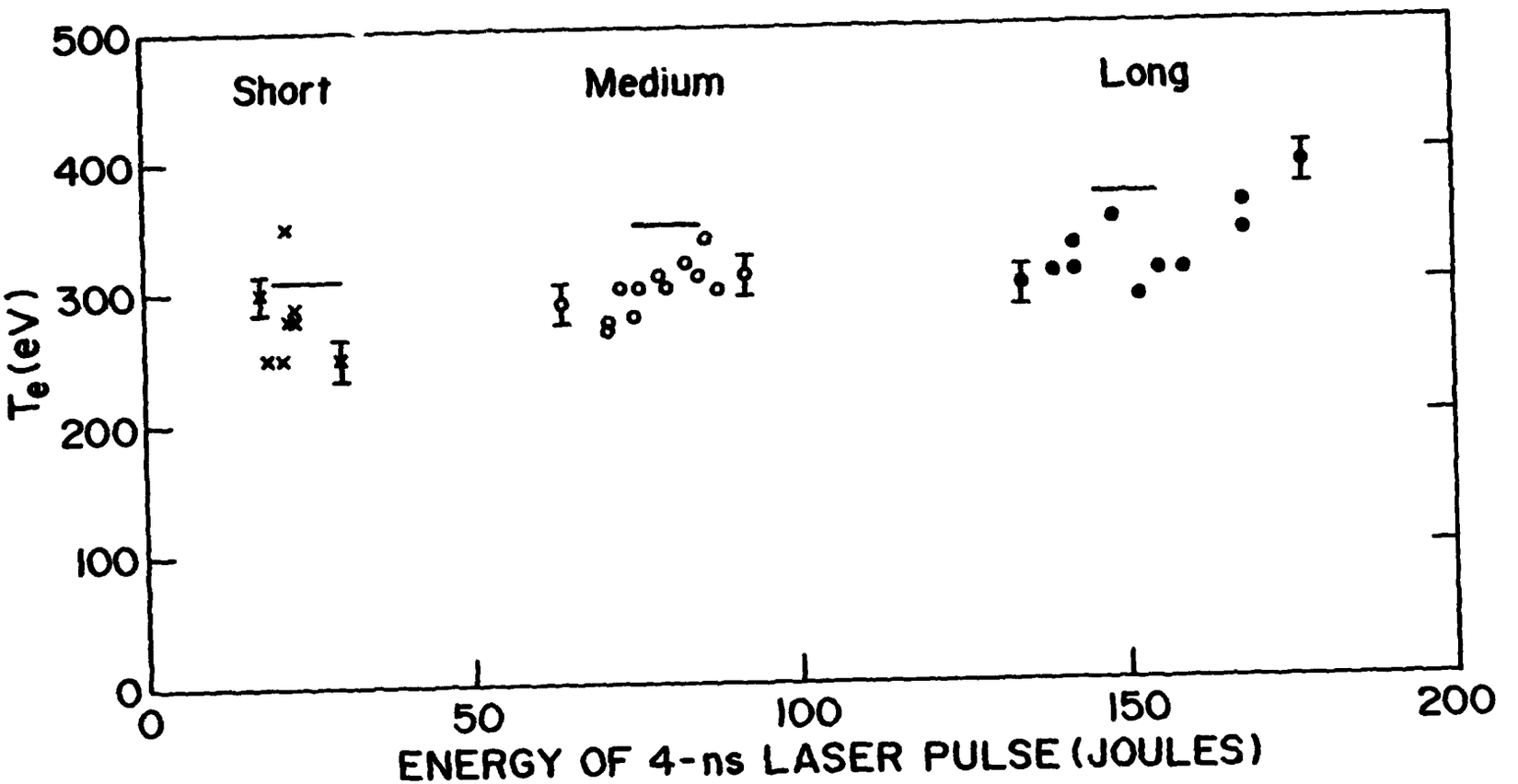

Fig. 4 Thermal electron temperatures from time-integrated spectra for the short, medium and long scalelengths. The time-resolved background temperatures from Fig. 2 are indicated by horizontal lines.

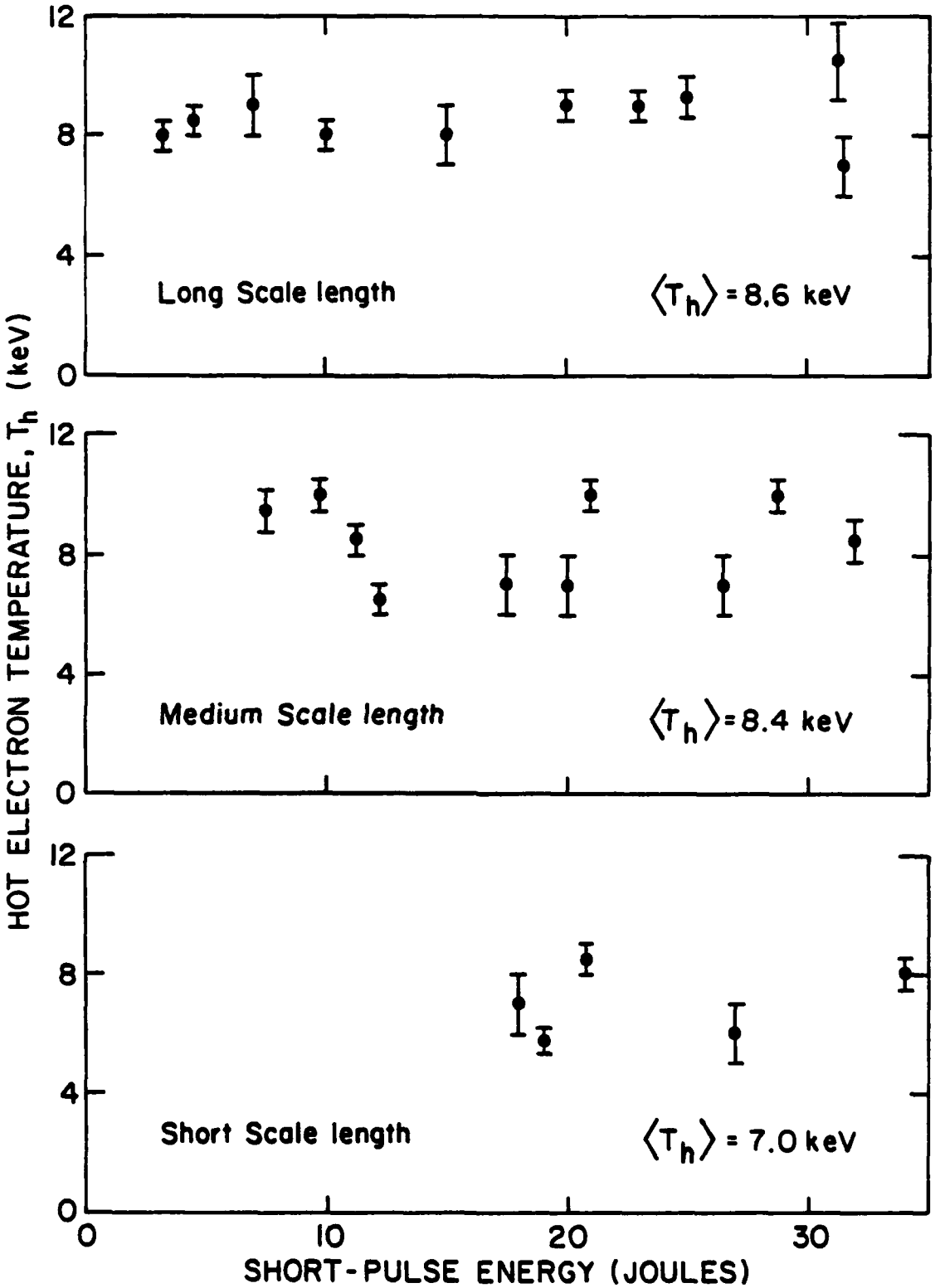

Fig. 5 Hot electron temperatures deduced from high energy (20-50 keV) x-ray spectral measurements for short, medium and long scalelength plasmas.

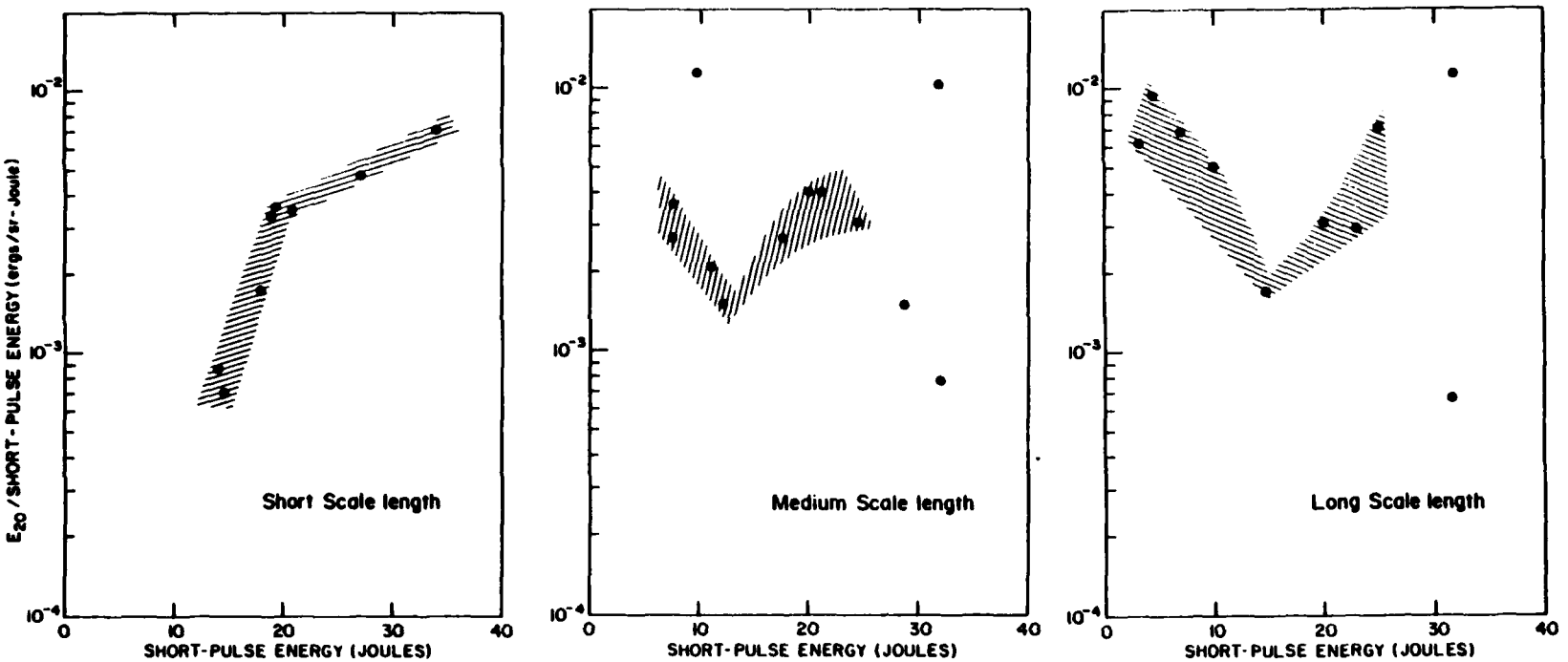

Fig. 6 Integrated intensities of x-rays above 20 keV, normalized to the incident short-pulse laser energy for short, medium and long scalelength plasmas.

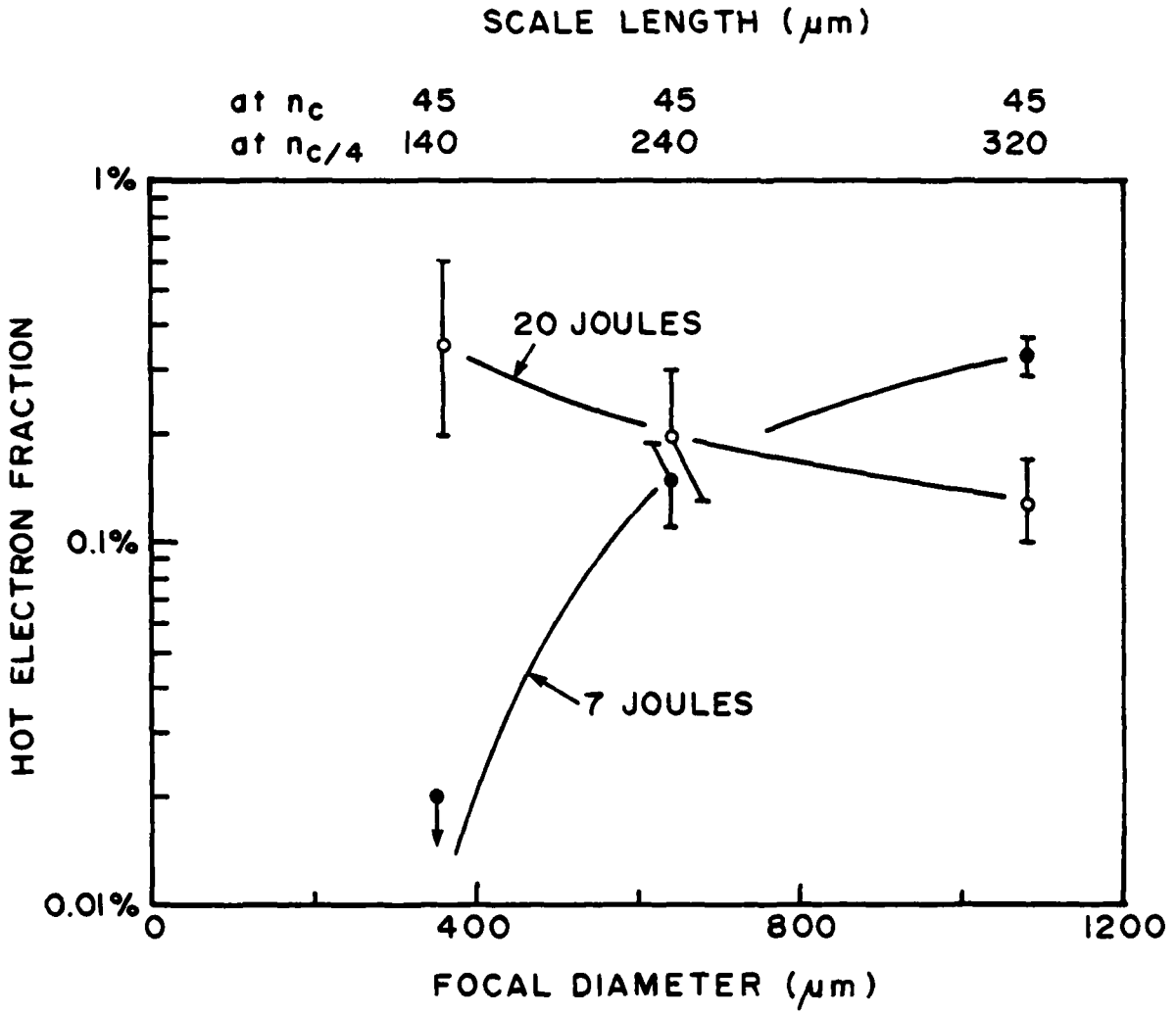

Fig. 7 Hot electron fractions determined from x-ray measurements as a function of the long-pulse focal diameter. Scalelengths corresponding to the short, medium and long scalelength conditions are given at the top of the figure. The data point of 7 Joules and short scalelength is an upper limit.

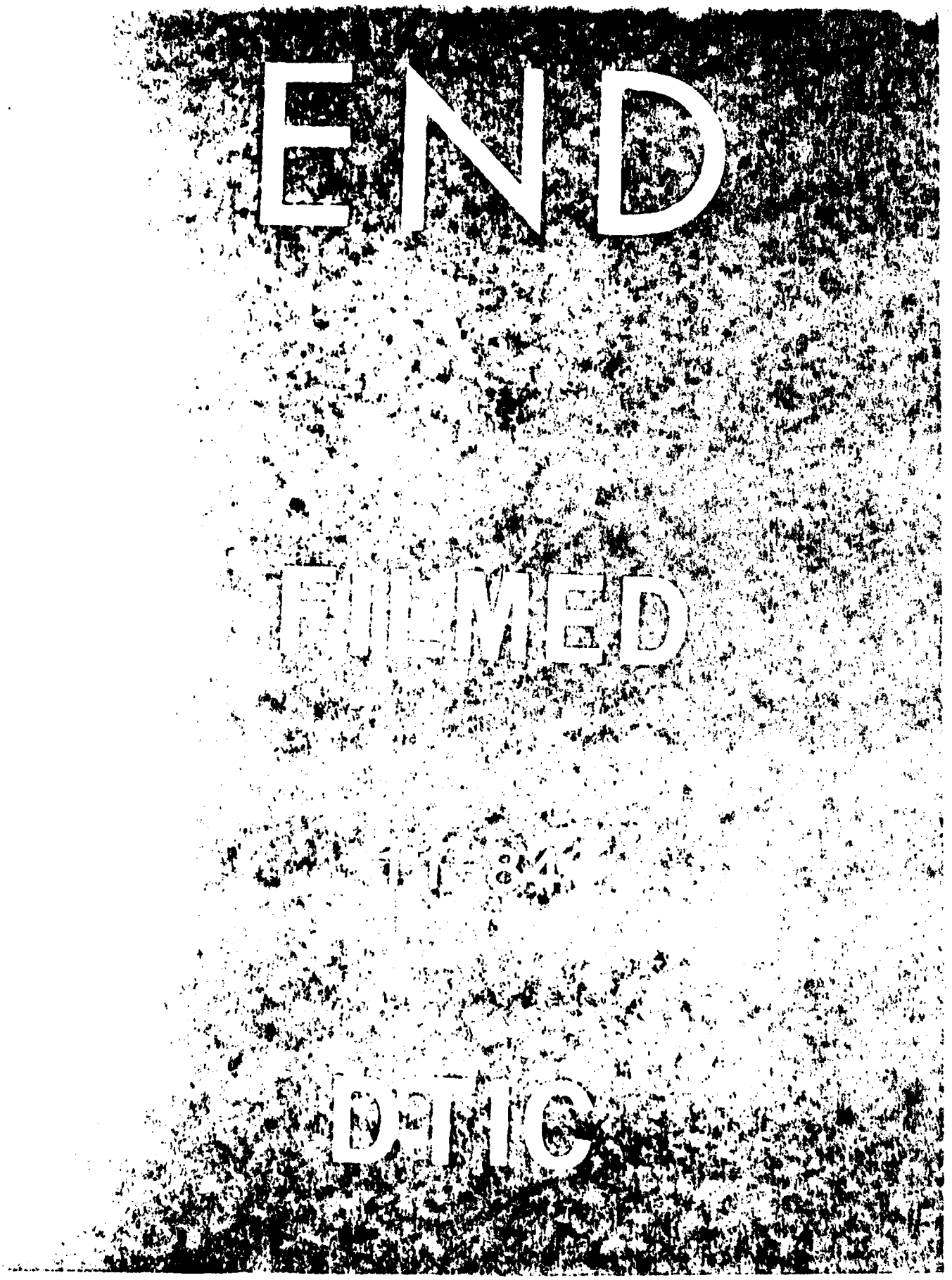
END
FILMED
DTIC